Review of Scientific Instruments ARTICLE scitation.org/journal/rsi

Scanning SQUID microscopy in a cryogen-free cooler

Cite as: Rev. Sci. Instrum. 90, 053702 (2019); doi: 10.1063/1.5087060
Submitted: 27 December 2018 • Accepted: 7 April 2019 •
Published Online: 16 May 2019

Yishai Shperber,[1,a),b)] Naor Vardi,[1,a)] Eylon Persky,[1] Shai Wissberg,[1] Martin E. Huber,[2] and Beena Kalisky[1]

AFFILIATIONS

[1] Department of Physics and Institute of Nanotechnology and Advanced Materials, Bar-Ilan University, Ramat-Gan, Israel
[2] Departments of Physics and Electrical Engineering, University of Colorado Denver, Denver, Colorado 80217, USA

[a)] **Contributions:** Y. Shperber and N. Vardi contributed equally to this work.
[b)] **Author to whom correspondence should be addressed:** Yishai.Shperber@biu.ac.il

ABSTRACT

Scanning superconducting quantum interference device (SQUID) microscopy is a powerful tool for investigating electronic states at surfaces and interfaces by mapping their magnetic signal. SQUID operation requires cryogenic temperatures, which are typically achieved by immersing the cryostat in liquid helium. Making a transition to cryogen free systems is desirable, but has been challenging, as electric noise and vibrations are increased in such systems. We report on the successful operation of a scanning SQUID microscope in a modified Montana Instruments cryogen-free cooler with a base temperature of 4.3 K. We demonstrate scanning SQUID measurements with flux noise performance comparable to a wet system and correlate the sensor-sample vibrations to the cryocooler operation frequencies. In addition, we demonstrate successful operation in a variety of SQUID operation modes, including mapping static magnetic fields, measurement of local susceptibility, and spatial mapping of current flow distribution.

INTRODUCTION

The scanning superconducting quantum interference device (SQUID) microscope (SSM) is a highly sensitive device for imaging magnetic flux distributions near surfaces. This powerful technique[1–9] can be applied to study local magnetic properties of materials,[10–19] as well as to obtain local maps of current distribution[20–25] and superconductivity.[26–34] Existing SSM systems are traditionally housed in a vacuum cryostat cooled by a thermal bath immersed in a "wet" liquid ^{4}He Dewar, or mounted on a dilution refrigerator mixing chamber. As the availability of ^{4}He decreases, and helium prices increase, more measurement techniques convert to "dry" operation.

Particularly, where scanning probe microscopy is concerned, the transition to dry operation is challenging. The cryocoolers typically operate at low frequencies, subjecting the microscope to increased electric noise and mechanical vibrations compared to its wet counterpart. Furthermore, the limited cooling power requires additional design considerations to obtain operation at base temperature.

Several cryogenic scanning probe techniques were successfully converted to dry technology [such as atomic force microscopy (AFM), magnetic force microscopy (MFM), scanning gate microscopy,[35] and scanning tunneling microscopy (STM)[37]]. These systems enjoy the capability to perform long measurements without the need to renew the helium bath. The critical challenge in these developments was to isolate the sensor-sample stage from the cold-head's mechanical vibrations. In this work, we describe the integration of a SQUID sensor, which is highly sensitive to electrical noise and grounding issues. In addition, the mechanical vibrations of the low impedance wiring also produce electrical noise through microphonic pickup.

We demonstrate SSM measurements in a Montana instruments Nanoscale-Workstation table-top system,[38] modified to host our microscope. We describe the modifications made to improve the sensor's electrical noise and sample base temperature, characterize the sensor-sample vibrations, and analyze the system's performance. We achieve a noise spectrum that is comparable to SQUIDs operated in liquid helium based cryostats. We demonstrate the capabilities of our dry SSM by examining vortices, local susceptibility maps, and

the spatial distributions of currents in normal and superconducting samples.

SYSTEM DESCRIPTION

We integrated our SSM in a Nanoscale-Workstation system of Montana Instruments stationed on an optical breadboard [unfloated optical table, Fig. 1(a)]. The system has two cold stages, kept at constant temperatures (4.3 K, 33 K) when operational. The 4.3 K stage hosts a wide, 197 mm, gold-plated copper platform. The 33 K stage includes an aluminum casing surrounding the 4 K stage, serving as a radiation shield, and the room for thermal clamping of wires [Fig. 1(b)]. We mount the microscope at the center of the 4 K stage. The height of the chamber was modified to 120 mm to host our microscope [Figs. 1(c) and 1(d)]. Using the Nanoscale-Workstation results in a table-top SSM, with convenient access to inner parts of the microscope. By removing the case [Figs. 1(b)–1(d)], the sensor-sample alignment can be performed inside the system, on the optical breadboard.

Figure 2(a) shows a schematic sketch of the microscope. The body of the microscope is made of oxygen free, high thermal conductivity (OFHC) copper, and its bottom is clamped to the 4 K platform using screws. To maximize the accessible scanning area, we combine coarse motion over a few millimeters with a fine scanning area of a few hundreds of microns. The coarse motion is performed by an Attocube stack of XYZ stick slip translation stages, covering an area of 5×5 mm^2. The fine scanning is performed by an in-house fabricated S-bender scanner, which allows a large linear scanning

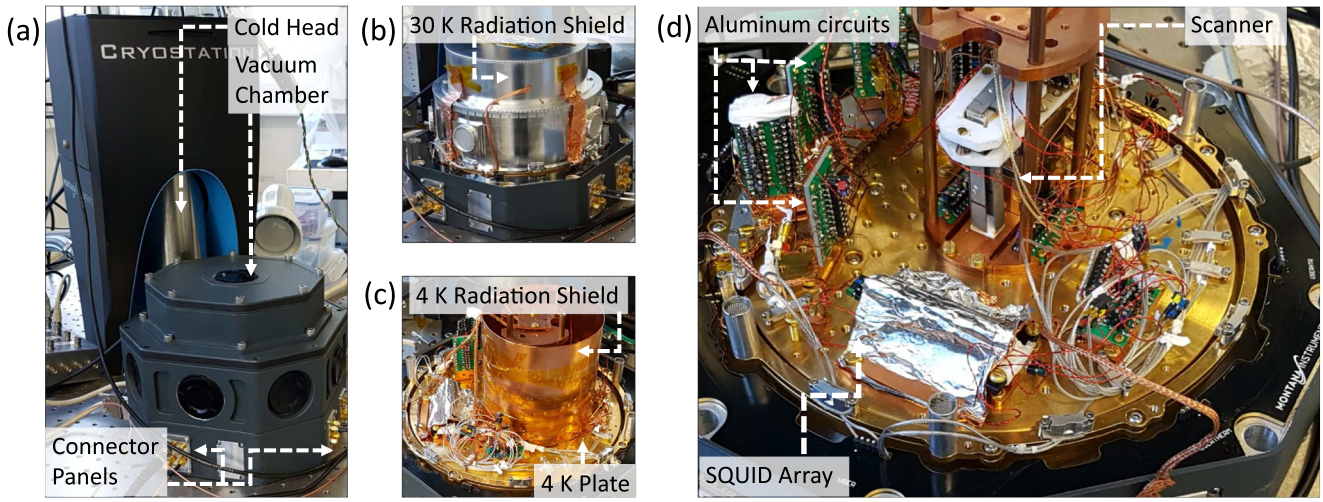

FIG. 1. The integrated cryogen-free SSM system. (a) The modified vacuum chamber and cold head stationed on an optical table. The table serves as the electrical ground for the system. (b) The vacuum case removed, showing the 30 K radiation shield and oxygen free copper braids (with cross section area of 1.27 mm^2 and length of 15 cm) used for thermal anchoring. (c) The system with the 30 K radiation shield removed. Visible are the scanner, the 4 K radiation shield, the measurement electronics, and the 4 K plate. (d) The scanner is stationed in the middle of the 4 K plate, next to the SQUID array (shielded by mu-metal, Nb, Cu, Pb, and Al sheets). The wires are thermally anchored by aluminum circuit boards at the 4 K and 30 K stages.

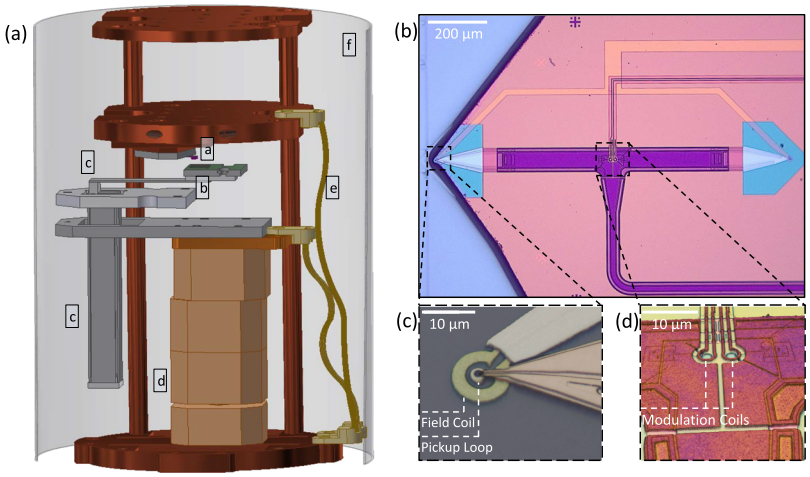

FIG. 2. The Scanning SQUID microscope. (a) CAD image of the cage and scanner, showing the following: a—the SQUID, b—the sample, c—S-bender piezoelectric plates for fine movement, d—coarse motion translation stages, e—oxygen-free copper braid for thermal anchoring, and f—copper radiation shield. (b) An optical image of the SQUID probe, showing the gradiometric design, with two pickup loops, modulation coils, and field coils. The chip is polished so that one pick up loop is near the edge of the chip. (c) A zoom in on the sensing point, showing the pickup loop surrounded by the field coil. (d) A zoom in on the modulation coils. Images (c) and (d) were taken using an optical profilometer by Zeta Instruments.

area of 500 × 500 μm^2 at base temperature.[39,40] It is built out of two pairs of S-bender piezoelectric plates for moving along the x-y plane and another perpendicular plate that allows movement in the z-direction [Fig. 2(a)].

The SQUID is a magnetic flux to voltage converter, combining the phenomena of flux quantization in superconductors and the Josephson effect to create a highly sensitive magnetometer.[41] Our SQUIDs are fabricated on a silicon chip in a multilayer Nb structure with Nb/AlOx/Nb junctions, following the design described in Ref. 3. The SQUID contains a pickup loop with a diameter of ~1 μm, modulation coils for improved sensitivity in a flux-locked loop, and a local field coil which enables susceptibility measurements [Figs. 2(b)–2(d)]. The SQUID signal is enhanced by a series array of 100 SQUIDs that acts as a cold amplifier,[42,43] which in turn is connected to room temperature electronics.

The SQUID chip is mounted on a cantilever made out of a thin 12 × 3 × 0.13 mm^3 copper sheet. We place the cantilever close to another conducting plate and continuously monitor the capacitance between the plates. The capacitance reading can be used for detecting contact while approaching the sample and for sensing the surface in order to scan at a constant height. This reading can also be used to quantify the force while lightly pressing (up to 1 μN) the surface in experiments allowing scans in contact (see supplementary material S1).

The main challenges in incorporating the SSM into a dry cryostat are limited cooling power and increased electrical and mechanical noise, caused by the cryostat dry operation. Solutions typically used in wet systems are not feasible. The dry system is inherently coupled to noise sources, while a wet system can be placed in a remote basement, far from power-consuming and vibrating devices, to reduce electrical and mechanical noises. Below, we describe the modifications to the commercial dry cryostat in order to operate our SSM.

An important challenge in cryo-free systems is the limited cooling power. Because the SQUID chip is glued to a cantilever [Fig. 2(a)—label a] rather than to a thick copper plate, its signal wires are an important factor in its thermal anchoring. To thermally couple the SQUID to the cold plate, we used copper wires to connect the SQUID's carrier to aluminum thermal-clad circuit boards, mounted on the 4 K plate of the cryostat. To thermally anchor the signal wires and minimize the heat-load on the 4 K plate, we used 30 cm phosphor-bronze low thermal conductivity twisted pairs wires (AWG 32) and 30 cm stainless steel coaxial cables (1 GHz—Lakeshore AWG 29), anchored both to the 30 K stage and 4 K stage by thermally conducting circuit boards [Figs. 1(b)–1(d)]. We replaced all other printed circuit boards with thermally conducting boards, most importantly the cold amplifier chip (the SQUID array) board, which stays stably anchored to the base plate temperature. Additional thermal anchors were made using a dedicated OFHC flex-link, prepared by Montana-Instruments.[44] These highly conductive thermal flex-links connect the SQUID plate and the scanner to the 4 K platform plate [Fig. 2(a)]. Also, to avoid radiation heating we added, in addition to the system's 30 K shield, a copper shield around the entire microscope, which is also kept at the base temperature of 4.3 K [Fig. 1(c)].

The main challenge in integrating scanning SQUID in a closed loop cooling system is electrical noise. Due to the low impedance of the SQUIDs and associated circuitry, SQUIDs are extremely sensitive to electromagnetic interference and ground loops in their vicinity, making the cryostat's "housekeeping" electronics an obstacle for optimal operation. For quiet SQUID measurements in the dry system, we did the following: We connected all of our electronics to the same ground, together with the cryostat's ground. We operated all signal lines in single-ended mode. We added low pass filters (with a cutoff frequency of 5 MHz) to the DC lines, and replaced the original nonconductive panels of the RF feedthrough with aluminum panels [Figs. 1(a) and 1(b)], connecting all coax cables shields to the system's ground. Instead of using the built-in platform thermometer and controller, we integrated another silicon diode temperature sensor wired to a separate LakeShore controller. These steps improved the noise significantly (see supplementary material S2), enabling SSM measurements. In addition, a table-top cooling system allows using wires that are significantly shorter than the typical length used in wet systems or dry bottom-loading systems, which improves noise performance due to the smaller inductance. Figures 3(a) and 3(b) show noise spectra as measured in our modified system, featuring peaks at power line frequencies (50, 100 Hz), compressor (30 Hz), cold-head operation (70 Hz), and 1/f noise level in the low frequency regime. In the higher frequency regime (>100 Hz), the white noise is 0.7–2 $\mu\Phi_0/\sqrt{\text{Hz}}$, depending on the specific sensor, with peaks at frequencies that vary between cooldowns and depend on the specific configuration of the experiment [see the difference between Figs. 3(a) and 3(b)]. Such noise curves allow for susceptibility measurements with a noise level comparable to a wet SSM.[3]

A well known challenge of scanning measurements in cryogen-free systems is mechanical vibrations. The vibrations of the 4 K platform with respect to the optical table are 5 nm (peak to peak, measured at Montana Instruments). While low vibrations levels between the cold platform and the optical table are important for optical measurements, the relevant figure for piezo-based scanning probe microscopy is the sensor-sample vibrations level. Sensor-sample vibrations are affected not only by the platform's vibrations, but also by the microscope's structure. The high sensitivity of the SQUID to small changes in the magnetic field allows us to use the magnetometer itself as a probe of small modulations in the sensor-sample distance.[45]

We used the magnetic signal from a vortex in a type II superconductor to characterize the sensor-sample vibrations in our system. A time-averaged image of the magnetic flux is shown in the inset of Fig. 3(c). We obtained the spectral dependence of the signal by computing the Fourier transform (with respect to time) at each pixel. In the absence of vibrations, the spatial map for each frequency would be the SQUID's noise at that frequency and will not have any spatial structure. However, in the presence of sensor-sample vibrations at some frequency, the signal at that frequency will have a distinct spatial structure: the magnetic signal, $B_z(\mathbf{r},\omega)$ will be proportional to the vibration amplitude, $\mathbf{dr}(\omega)$, and to the spatial derivative of the DC signal, in the direction of the vibration.[45,46]

$$B_z(\boldsymbol{r},\omega) = \boldsymbol{dr}(\omega)\cdot\nabla_{\boldsymbol{r}}(B_z(\boldsymbol{r},\omega=0)).$$

We then fit the data to this equation, and recover the amplitude and frequency of the vibrations in our system for XYZ axes [Fig. 3(c)]. For most frequencies, the vibrations are less than 15 nm peak to peak. At some frequencies, associated with the pulse-tube operation

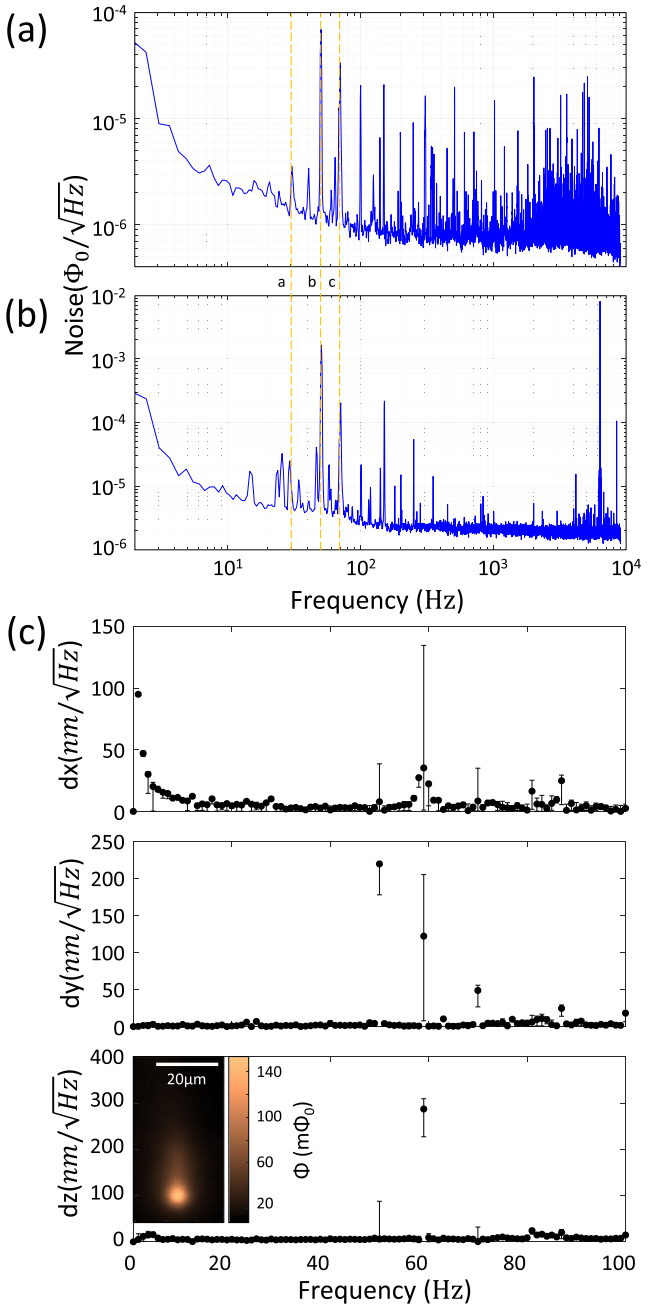

FIG. 3. Vibration and electrical noise characterization. [(a) and (b)] Flux noise measured by a scanning SQUID sensor in the cryogen-free system, in two different scanning configurations. The signal is measured as fractions of the magnetic flux quantum, Φ_0 (Φ_0 = h/2e). The spectrum, in a log-log scale, shows some characteristic peaks, such as a—compressor (30 Hz), b—network (50 Hz), c—cold-head operation (70 Hz), and an overall 1/f noise. The white noise and the peaks at higher frequencies change with every cooldown and are sample and experiment dependent. (c) Vibration amplitude in our system along different axes, as a function of frequency. Error bars are 95% confidence intervals, determined by statistical bootstrapping.[46] See the additional plot in the supplementary material S4. Inset: A time averaged image of the magnetic flux used in the analysis of the vibrations in the system.

(~1 Hz, 70 Hz), or with the power grid (50 Hz), we see an increased vibration level. The increased vibration level also exists at 60 Hz, possibly due to a mechanical resonance in our microscope.

In most scanning probe microscopy techniques, such as AFM, MFM, or STM, mechanical vibrations are the main obstacle in implementing the scanning capabilities in cryogen-free systems. This is due to their high sensitivity to the distance between the sensor and the sample, and the damage that can be inflicted upon the sensor from unwanted contact with the sample. It is possible to attenuate these vibrations, for example, by using springs and mass.[35,47] However, with limited cooling power of a dry system, we must balance thermal performance and the level of vibration isolation, and thus treat each configuration individually. In our setup, with micron-scale resolution, the vibration levels reported here [Fig. 3(c)] are sufficient. In addition, the robustness of the SQUID chip allows for scanning in contact, which dramatically reduces sample-sensor vibrations for measurements where the SQUID and the sample temperatures are the same. For higher spatial resolution, with nanoscale pickup loop sizes, further vibration isolation steps are required to reduce the vibration level, as reported in Ref. 47.

In addition to sample-sensor distance, mechanical vibrations can induce electrical noise in the SQUID through microphonic pickup. In order to separate the contributions of mechanical and electrical vibrations to the SQUID's flux noise, we electrically connected a wet system (not coupled to mechanical vibrations from the cold head) to the cryogen-free system. We found that the main contribution to the SQUID noise is electrical rather than mechanical (see supplementary material S3).

DEMONSTRATION OF DRY-SSM MEASUREMENT CAPABILITIES

Our SQUID can measure several properties simultaneously: magnetism, susceptibility, and 2D current distribution. To demonstrate these capabilities in our dry system, we imaged the following samples: a 70 nm thick steel meander evaporated on Si [Fig. 4(a)]; a 30 nm thick NbN film evaporated on $SrTiO_3$ (STO); 5 unit cells of $LaAlO_3$ (LAO) grown on STO; and a 150 nm thick Nb film evaporated on Al_2O_3.

The steel sample was cooled in zero field to form an inhomogeneous, complicated magnetic landscape. Figure 4(b) shows a map of the DC magnetic signal, where the meander is filled with small, resolution-limited, magnetic moments (magnetic domains of iron). Figure 4(c) shows a magnetometry image of superconducting vortices in NbN/STO. Some flux is found in straight lines, which are aligned with the crystallographic directions of the substrate due to the presence of structural domain walls in the STO.[33]

Next, we used the same steel sample to image the current flow in the steel meander. We drive bias current of 10 μA rms at 1904 Hz through the meander. We used a lock-in amplifier to record the magnetic field generated by the current flow [Fig. 4(d)]. Measuring the signal generated by the AC current allowed us to simultaneously map it with the DC magnetism, while avoiding the 1/f noise of our sensor.

Figures 4(e) and 4(f) show maps of the spatial distribution of the current flow at the conducting interface of LAO/STO. The maps reveal an inhomogeneous flow of current [Fig. 4(e)] and current flow that is directed along domain walls in the STO [Fig. 4(f)].[22,48]

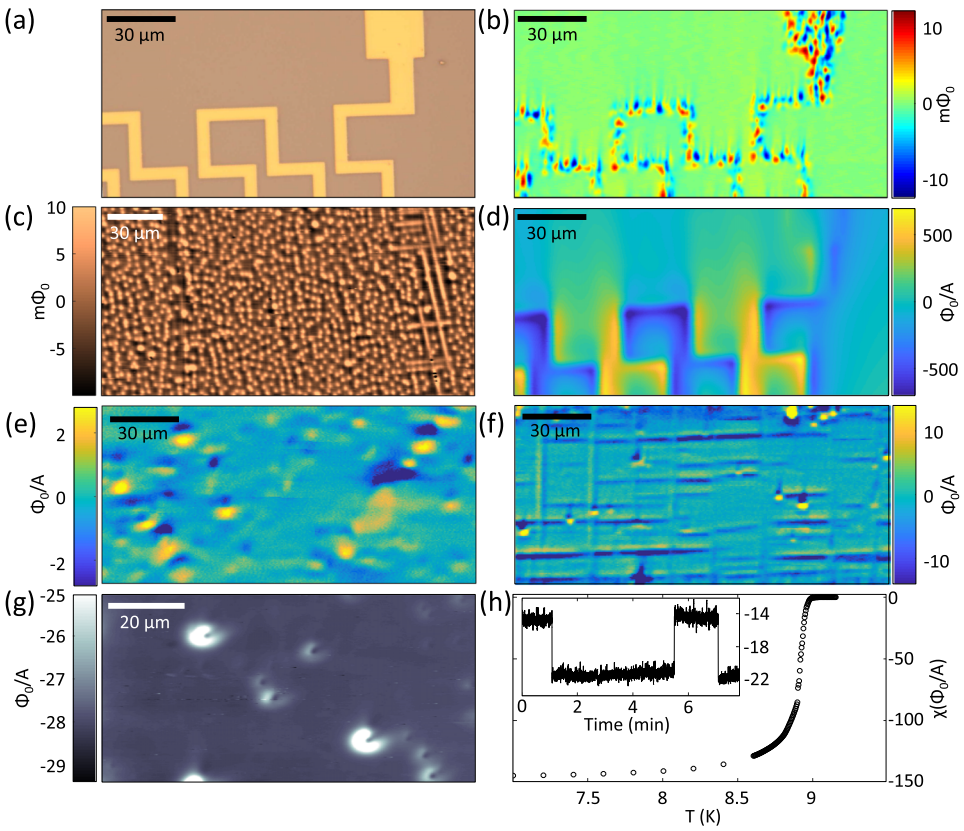

FIG. 4. Different measurements performed by the SSM. (a) Optical image of the steel meander measured by our SSM. (b) DC magnetic map of the steel meander, showing the different magnetic domains. (c) Magnetic image of vortices in NbN/STO. (d) Image of the magnetic field generated by the current flow in the meander. [(e) and (f)] Magnetic field generated by the current flow in LAO/STO, showing (e) current holes as dipoles, and (f) domain walls as vertical and horizontal stripes. (g) Susceptibility map recorded over NbN/STO, showing areas of reduced superconductivity. (h) Susceptibility measurements as a function of temperature, showing a decay of the diamagnetic response toward T_C of 8.95 K. Inset: Fluctuations of the susceptibility signal measured at constant temperature of 8.92 K.

The SQUID can also detect local magnetic susceptibility by applying a local magnetic field with the on-chip field coil.[33,49] Through this functionality, it can record paramagnetic signals near localized spins or the diamagnetic response near the surface of a superconductor. Figure 4(g) shows a susceptibility map measured on a NbN film, superconducting below 12 K. The diamagnetic response shows areas of reduced superconductivity due to small defects.[50]

Finally, on Nb/Al_2O_3, we performed susceptibility measurements as a function of temperature and recorded the monotonic decrease of the susceptibility to zero [Fig. 4(h)], with a critical temperature of 8.95 K. The dry cryostat offers a high degree of temperature stability over long periods of time, allowing us to measure the time dependence of the susceptibility at fixed temperatures. Near the critical temperature, we observe thermal fluctuations in the superconductivity as quantized changes to the diamagnetic response, as shown in the inset of Fig. 4(h).[49]

CONCLUSIONS

To conclude, we have integrated a scanning SQUID microscope in a cryogen-free environment. We made several modifications to a commercially available system, reducing the sensor's noise and improving the thermal coupling of the sensor and sample to the 4 K platform. We demonstrated the scanning and measuring capabilities by mapping magnetic topographies, as well as current response and magnetic susceptibility. The procedures described here can assist the integration of other low noise techniques where transition to dry operation is desired.

SUPPLEMENTARY MATERIAL

Supplementary material includes more information about the flux-noise and the capacitance surface sensing.

ACKNOWLEDGMENTS

We thank Kerry Neal, Caleb Schreibeis, and Brian Smithgall from Montana Instruments and Ilya Sochnikov from UCONN for fruitful discussions. We thank Y. Abulafia for assistance with the measurements and analysis. We thank A. Sharoni for providing NbN films and H. Y. Hwang for LAO/STO samples. This research was supported by the European Research Council Grant No. ERC-2014-STG-639792, the Israeli Science Foundation Grant No. ISF-1281/17, COST Action CA16218, and the QuantERA ERA-NET Cofund in Quantum Technologies (Project No. 731473).

REFERENCES

[1] J. R. Kirtley, M. B. Ketchen, C. C. Tsuei, J. Z. Sun, W. J. Gallagher, L. S. Yu-Jahnes, A. Gupta, K. G. Stawiasz, and S. J. Wind, IBM J. Res. Dev. **39**, 655 (1995).
[2] J. R. Kirtley and J. P. Wikswo, Annu. Rev. Mater. Sci. **29**, 117 (1999).
[3] M. E. Huber, N. C. Koshnick, H. Bluhm, L. J. Archuleta, T. Azua, P. G. Björnsson, B. W. Gardner, S. T. Halloran, E. A. Lucero, and K. A. Moler, Rev. Sci. Instrum. **79**, 053704 (2008).

[4]N. C. Koshnick, M. E. Huber, J. A. Bert, C. W. Hicks, J. Large, H. Edwards, and K. A. Moler, Appl. Phys. Lett. **93**, 243101 (2008).
[5]A. Finkler, D. Vasyukov, Y. Segev, L. Ne'eman, E. O. Lachman, M. L. Rappaport, Y. Myasoedov, E. Zeldov, and M. E. Huber, Rev. Sci. Instrum. **83**, 073702 (2012).
[6]D. Vasyukov, Y. Anahory, L. Embon, D. Halbertal, J. Cuppens, L. Neeman, A. Finkler, Y. Segev, Y. Myasoedov, M. L. Rappaport, M. E. Huber, and E. Zeldov, Nat. Nanotechnol. **8**, 639 (2013).
[7]J. R. Kirtley, L. Paulius, A. J. Rosenberg, J. C. Palmstrom, C. M. Holland, E. M. Spanton, D. Schiessl, C. L. Jermain, J. Gibbons, Y.-K.-K. Fung, M. E. Huber, D. C. Ralph, M. B. Ketchen, G. W. Gibson, Jr., and K. A. Moler, Rev. Sci. Instrum. **87**, 093702 (2016).
[8]C. Granata and A. Vettoliere, Phys. Rep. **614**, 1 (2016).
[9]F. Foroughi, J.-M. Mol, T. Müller, J. R. Kirtley, K. A. Moler, and H. Bluhm, Appl. Phys. Lett. **112**, 252601 (2018).
[10]J. R. Kirtley, Supercond. Sci. Technol. **22**, 064008 (2009).
[11]B. Kalisky, J. A. Bert, B. B. Klopfer, C. Bell, H. K. Sato, M. Hosoda, Y. Hikita, H. Y. Hwang, and K. A. Moler, Nat. Commun. **3**, 922 (2012).
[12]J. O. Walbrecker, B. Kalisky, D. Grombacher, J. Kirtley, K. A. Moler, and R. Knight, J. Magn. Reson. **242**, 10 (2014).
[13]E. O. Lachman, A. F. Young, A. Richardella, J. Cuppens, H. R. Naren, Y. Anahory, A. Y. Meltzer, A. Kandala, S. Kempinger, Y. Myasoedov, M. E. Huber, N. Samarth, and E. Zeldov, Sci. Adv. **1**, e1500740 (2015).
[14]X. R. Wang, C. J. Li, W. M. Lü, T. R. Paudel, D. P. Leusink, M. Hoek, N. Poccia, A. Vailionis, T. Venkatesan, J. M. D. Coey, E. Y. Tsymbal, Ariando, and H. Hilgenkamp, Science **349**, 716 (2015).
[15]A. Kremen, S. Wissberg, N. Haham, E. Persky, Y. Frenkel, and B. Kalisky, Nano Lett. **16**, 1626 (2016).
[16]A. Noguchi, H. Oda, Y. Yamamoto, A. Usui, M. Sato, and J. Kawai, Geophys. Res. Lett. **44**, 5360, https://doi.org/10.1002/2017gl073201 (2017).
[17]P. Reith, X. Renshaw Wang, and H. Hilgenkamp, Rev. Sci. Instrum. **88**, 123706 (2017).
[18]D. Vasyukov, L. Ceccarelli, M. Wyss, B. Gross, A. Schwarb, A. Mehlin, N. Rossi, G. Tütüncüoglu, F. Heimbach, R. R. Zamani, A. Kovács, A. Fontcuberta i Morral, D. Grundler, and M. Poggio, Nano Lett. **18**, 964 (2018).
[19]D. V. Christensen, Y. Frenkel, Y. Z. Chen, Y. W. Xie, Z. Y. Chen, Y. Hikita, A. Smith, L. Klein, H. Y. Hwang, N. Pryds, and B. Kalisky, Nat. Phys. **15**, 269–274 (2019).
[20]S. Chatraphorn, E. F. Fleet, F. C. Wellstood, L. A. Knauss, and T. M. Eiles, Appl. Phys. Lett. **76**, 2304 (2000).
[21]K. C. Nowack, E. M. Spanton, M. Baenninger, M. König, J. R. Kirtley, B. Kalisky, C. Ames, P. Leubner, C. Brüne, H. Buhmann, L. W. Molenkamp, D. Goldhaber-Gordon, and K. A. Moler, Nat. Mater. **12**, 787 (2013).
[22]B. Kalisky, E. M. Spanton, H. Noad, J. R. Kirtley, K. C. Nowack, C. Bell, H. K. Sato, M. Hosoda, Y. Xie, Y. Hikita, C. Woltmann, G. Pfanzelt, R. Jany, C. Richter, H. Y. Hwang, J. Mannhart, and K. A. Moler, Nat. Mater. **12**, 1091 (2013).
[23]N. Shadmi, A. Kremen, Y. Frenkel, Z. J. Lapin, L. D. Machado, S. B. Legoas, O. Bitton, K. Rechav, R. Popovitz-Biro, D. S. Galvão, A. Jorio, L. Novotny, B. Kalisky, and E. Joselevich, Nano Lett. **16**, 2152 (2016).
[24]Y. Frenkel, N. Haham, Y. Shperber, C. Bell, Y. Xie, Z. Chen, Y. Hikita, H. Y. Hwang, and B. Kalisky, ACS Appl. Mater. Interfaces **8**, 12514 (2016).
[25]D. Halbertal, M. Ben Shalom, A. Uri, K. Bagani, A. Y. Meltzer, I. Marcus, Y. Myasoedov, J. Birkbeck, L. S. Levitov, A. K. Geim, and E. Zeldov, Science **358**, 1303 (2017).
[26]D. A. Wollman, D. J. Van Harlingen, W. C. Lee, D. M. Ginsberg, and A. J. Leggett, Phys. Rev. Lett. **71**, 2134 (1993).
[27]B. L. T. Plourde, D. J. Van Harlingen, N. Saha, R. Besseling, M. B. S. Hesselberth, and P. H. Kes, Phys. Rev. B **66**, 054529 (2002).
[28]N. C. Koshnick, H. Bluhm, M. E. Huber, and K. A. Moler, Science **318**, 1440 (2007).
[29]B. Kalisky, J. R. Kirtley, J. G. Analytis, J.-H. Chu, A. Vailionis, I. R. Fisher, and K. A. Moler, Phys. Rev. B **81**, 184513 (2010).
[30]J. A. Bert, K. C. Nowack, B. Kalisky, H. Noad, J. R. Kirtley, C. Bell, H. K. Sato, M. Hosoda, Y. Hikita, H. Y. Hwang, and K. A. Moler, Phys. Rev. B **86**, 060503 (2012).
[31]J. R. Kirtley, B. Kalisky, J. A. Bert, C. Bell, M. Kim, Y. Hikita, H. Y. Hwang, J. H. Ngai, Y. Segal, F. J. Walker, C. H. Ahn, and K. A. Moler, Phys. Rev. B **85**, 224518 (2012).
[32]L. Embon, Y. Anahory, Ž. L. Jelić, E. O. Lachman, Y. Myasoedov, M. E. Huber, G. P. Mikitik, A. V. Silhanek, M. V. Milošević, A. Gurevich, and E. Zeldov, Nat. Commun. **8**, 85 (2017).
[33]S. Wissberg and B. Kalisky, Phys. Rev. B **95**, 144510 (2017).
[34]A. Kremen, H. Khan, Y. L. Loh, T. I. Baturina, N. Trivedi, A. Frydman, and B. Kalisky, Nat. Phys. **14**, 1205 (2018).
[35]M. Pelliccione, A. Sciambi, J. Bartel, A. J. Keller, and D. Goldhaber-Gordon, Rev. Sci. Instrum. **84**, 033703 (2013).
[36]F. P. Quacquarelli, J. Puebla, T. Scheler, D. Andres, C. Bödefeld, B. Sipos, C. D. Savio, A. Bauer, C. Pfleiderer, A. Erb, and K. Karrai, Microsc. Today **23**, 12 (2015).
[37]A. M. J. den Haan, G. H. C. J. Wijts, F. Galli, O. Usenko, G. J. C. van Baarle, D. J. van der Zalm, and T. H. Oosterkamp, Rev. Sci. Instrum. **85**, 035112 (2014).
[38]See https://www.montanainstruments.com/Products/Cryostation for more details about the Cryostation.
[39]J. Siegel, J. Witt, N. Venturi, and S. Field, Rev. Sci. Instrum. **66**, 2520 (1995).
[40]P. G. Björnsson, B. W. Gardner, J. R. Kirtley, and K. A. Moler, Rev. Sci. Instrum. **72**, 4153 (2001).
[41]J. Clarke and A. I. Braginski, *The SQUID Handbook: Fundamentals and Technology of SQUIDs and SQUID Systems* (John Wiley & Sons, 2006).
[42]R. P. Welty and J. M. Martinis, IEEE Trans. Magn. **27**, 2924 (1991).
[43]M. E. Huber, P. A. Neil, R. G. Benson, D. A. Burns, A. F. Corey, C. S. Flynn, Y. Kitaygorodskaya, O. Massihzadeh, J. M. Martinis, and G. C. Hilton, IEEE Trans. Appl. Supercond. **11**, 4048 (2001).
[44]L. R. Mauritsen, M. B. Simmonds, and D. Griffing, U.S. patent 9303914 (5 April 2016).
[45]D. Schiessl, J. R. Kirtley, L. Paulius, A. J. Rosenberg, J. C. Palmstrom, R. R. Ullah, C. M. Holland, Y.-K.-K. Fung, M. B. Ketchen, G. W. Gibson, and K. A. Moler, Appl. Phys. Lett. **109**, 232601 (2016).
[46]E. Persky, N. Vardi, Y. Shperber, and B. Kalisky, Appl. Phys. Lett. **113**, 173101 (2018).
[47]L. Bishop-Van Horn, Z. Cui, J. R. Kirtley, and K. A. Moler, e-print arXiv: 1812.03215 (2018).
[48]Y. Frenkel, N. Haham, Y. Shperber, C. Bell, Y. Xie, Z. Chen, Y. Hikita, H. Y. Hwang, E. K. H. Salje, and B. Kalisky, Nat. Mater. **16**, 1203 (2017).
[49]S. Wissberg, A. Frydman, and B. Kalisky, Appl. Phys. Lett. **112**, 262602 (2018).
[50]H. Noad, C. A. Watson, H. Inoue, M. Kim, H. K. Sato, C. Bell, H. Y. Hwang, J. R. Kirtley, and K. A. Moler, Phys. Rev. B **98**, 064510 (2018).